

**RocFall2**

# **Lump Mass Fragmentation Analysis**

Verification Manual

# Table of Contents

<b>Introduction .....</b>	<b>3</b>
<b>1. Drop tests simulations .....</b>	<b>5</b>
1.1. Validation of the fragmentation survival probability .....	5
1.2. Validation of the mass, velocity and launch angle of the fragments .....	12
<b>2. Multi impact simulations .....</b>	<b>17</b>
2.1. Influence of Severity of the Second Impact ( <b>h1</b> fixed while <b>h2</b> variable) on the Survival Probability of the Second Impact .....	19
2.2. Influence of Severity of the First Impact ( <b>h1</b> variable while <b>h2</b> fixed) on the Survival Probability of the Second Impact .....	23
<b>3. In-situ tests simulations .....</b>	<b>26</b>
3.1. Comparison with in-situ observation .....	30
<b>References .....</b>	<b>32</b>

# Introduction

A combination of targeted simulations and sensitivity analyses is used to validate the integration of fragmentation model proposed by Guccione et al. 2025 into RocFall2. The detailed simulations program consists of:

1. **Drop tests simulations** were conducted to validate the fragmentation module against the experimental results reported by Guccione et al. (2021a, 2023). In line with the experimental campaigns, the impacted target in the simulations is a concrete slab, while the blocks are assigned the properties of three different rock-like (mortar) materials. This validation step includes *validation of the fragmentation survival probability* (see Section 1.1) and *validation of the mass, velocity and launch angle of the fragments* (see Section 1.2).
2. **Multi impact simulations.** A synthetic slope profile was used to illustrate the cumulative damage effects from multiple impacts in rockfall simulations by varying the height of the second impact (see Section 2.1) and by varying the height of the first impact (see Section 2.2).
3. **In-situ tests simulations.** For the last validation, in-situ tests conducted in Spain (Gili et al. 2022; Matas et al. 2020; Prades-Valls et al. 2022) were replicated and compared (where possible) (see Section 3).

To conduct analysis with the fragmentation module, the module needs to be activated on the project setting (see Figure 0-1). For verification purposes, note that the “Lower block mass threshold” needs to be set to the desired value and enable “Advanced rock type entry” to access advanced parameter entry for seeder rock type.

When conducting RocFall2 analysis using the fragmentation module, extra input parameters for the material characteristics need to be added for the slope and for the rock type (see Figure 0-2). Note that for the rock type, two entry options are available: simplified (Figure 0-2b) and advanced (Figure 0-2c).

Before the validation tests sections, a list of symbols is reported to help to familiarize with the new terms used in the fragmentation module.

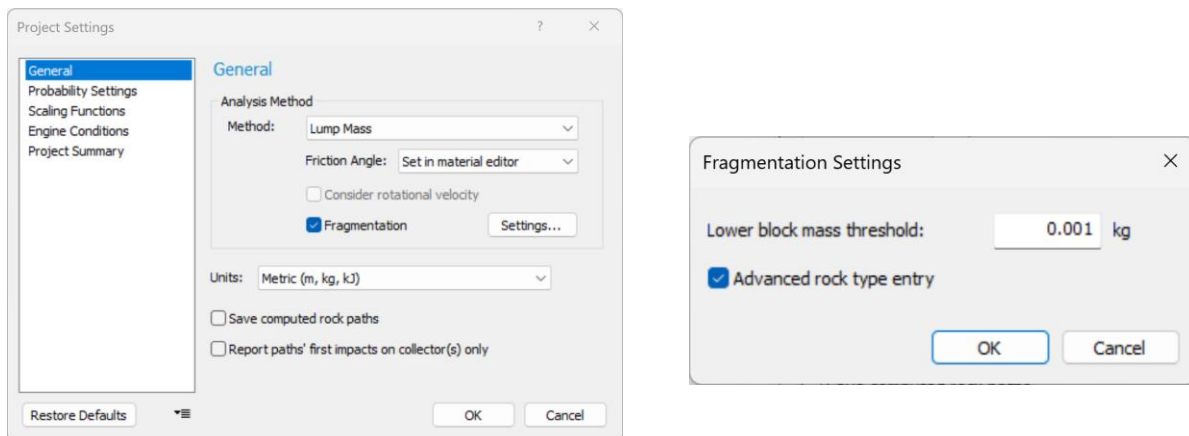


Figure 0-1 Project Settings: Analysis Method - Fragmentation

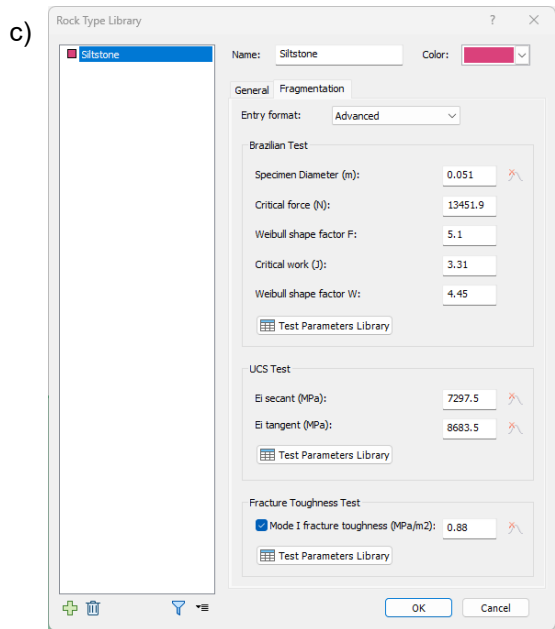
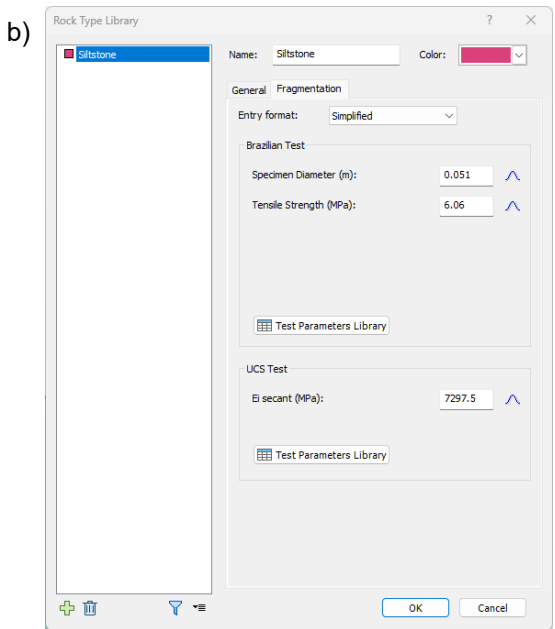
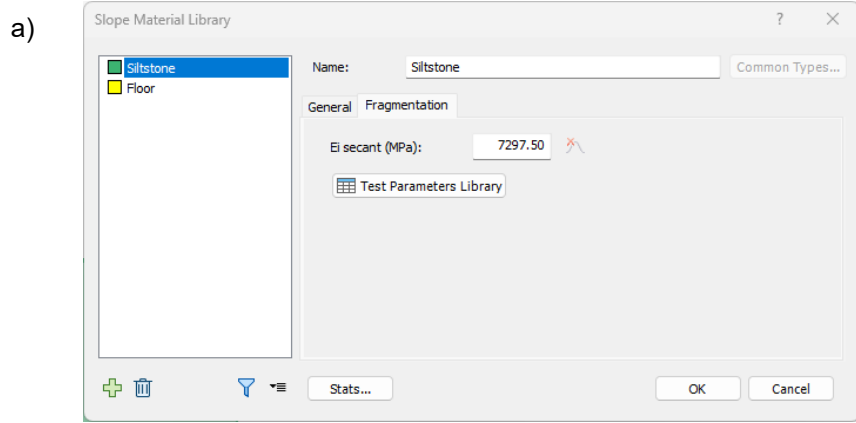


Figure 0-2 Fragmentation input parameters for slope a) and for the rock type: b) simplified and c) advanced option.

# 1. Drop tests simulations

---

[RocFall2 Build 8.027]

## 1.1. Validation of the fragmentation survival probability

Experimental survival probabilities were obtained from Guccione et al. (2021a) for three sphere diameters (50, 75, and 100 mm) and two materials (M1 and M2), based on 16 drop tests per impact velocity and five impact velocities per diameter. The general inputs parameters used for the four series of tests (S2 100 mm M1, S3 50 mm M2, S4 50 mm M2, and S5 100 mm M2) are reported in Figure 1-1. Both advanced and simplified fragmentation input configurations were tested. The specific parameters for materials M1 and M2 can be found in Figure 1-2a-b and Figure 1-2c-d, respectively. For this validation, “Lower block mass threshold” was set to 0.001 kg.

As mentioned in the introduction, the impacted surface (slope) was modeled as a concrete slab. General input parameters such as normal and tangential coefficient of restitutions and friction angle were based on experimental evidence during laboratory tests. These parameters are reported in Figure 1-3. Note the no distribution was applied to these parameters. Regarding the fragmentation parameter for the slab, the “Ei secant” was set to 11700 MPa as per Guccione et al. (2021b).

For validation purposes, 500 spheres were virtually dropped for each impact velocity within the survival probability range. A total of six impact velocities were selected for verification, including four matching the experimental series, as well as the survival velocity ( $v_{surv}$ ) and fragmentation velocity ( $v_{frag}$ ). The drop heights and corresponding impact velocities for each series are reported in Table 1-1, Table 1-2, Table 1-3 and Table 1-4. The profile and seeders used for the validation of fragmentation survival probability are illustrated in Figure 1-4.

Figure 1-5 illustrates the simulation results, in term of trajectories, for the validation of the fragmentation survival probability for the four series: a) 100 mm M1, b) 50 mm M2, c) 75 mm M2 and d) 100 mm M2, using the advanced input parameters.

Figure 1-6 presents the fragmentation survival probability as function of impact velocity, comparing experimental observations from Guccione et al. (2021a) with simulation results using both advanced and simplified input parameters. Each subfigure corresponds to a different test series: a) 100 mm M1, b) 50 mm M2, c) 75 mm M2 and d) S4 100 mm M2. In the experimental drop tests, each point represents 16 drop tests, while in the simulations, each point corresponds to 500 virtual drops. The lines represent the analytical prediction (see Guccione et al 2021a, 2025 for full derivation), plotted for both advanced and the simplified input configurations.

Simulation results fall within the expected error margins: using advanced input parameters, the deviation in impact velocity is less than -5% compared to the theoretical model. With simplified inputs, the error increases slightly, remaining below approximately -15%. Nonetheless, the simplified configuration still yields satisfactory agreement with the experimental data.

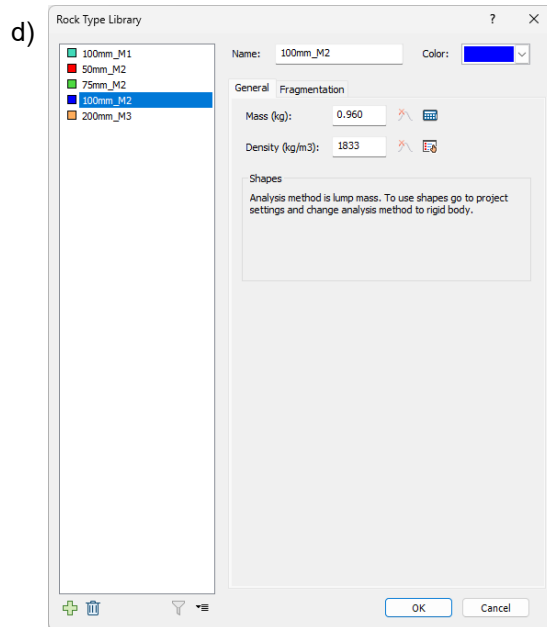
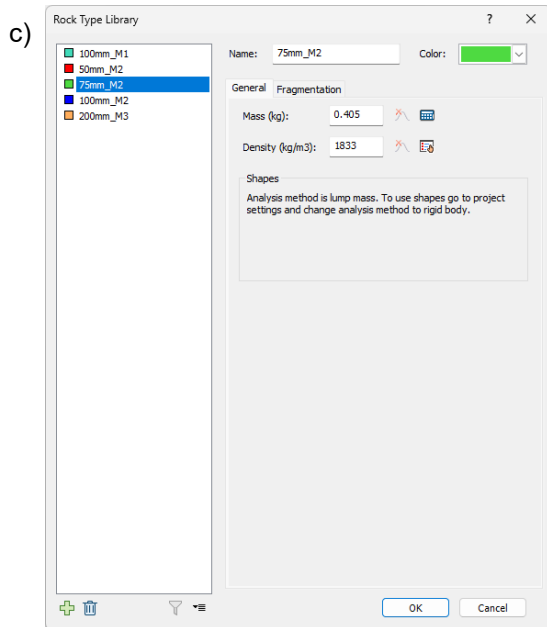
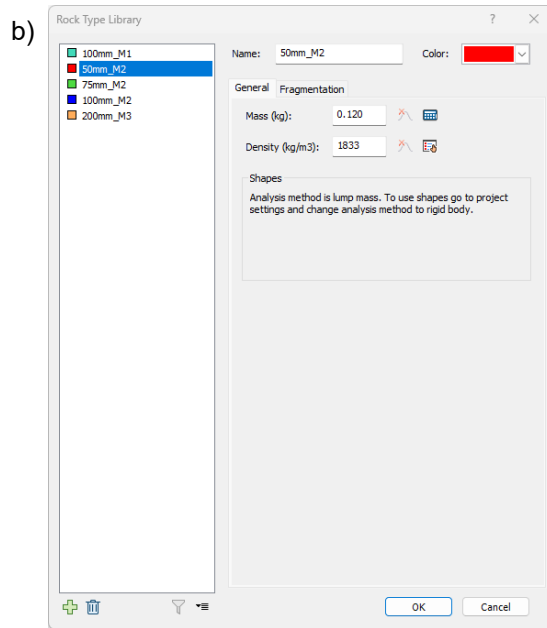
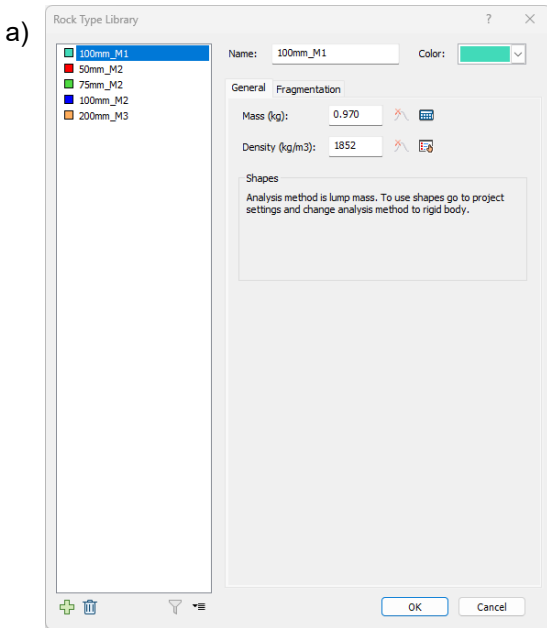


Figure 1-1 General parameters used for Validation Tests 1.1. Figure a) S2 (100 mm M1), b) S3 (50 mm M2), c) S4 (75 mm M2) and d) S5 (100 mm M2).

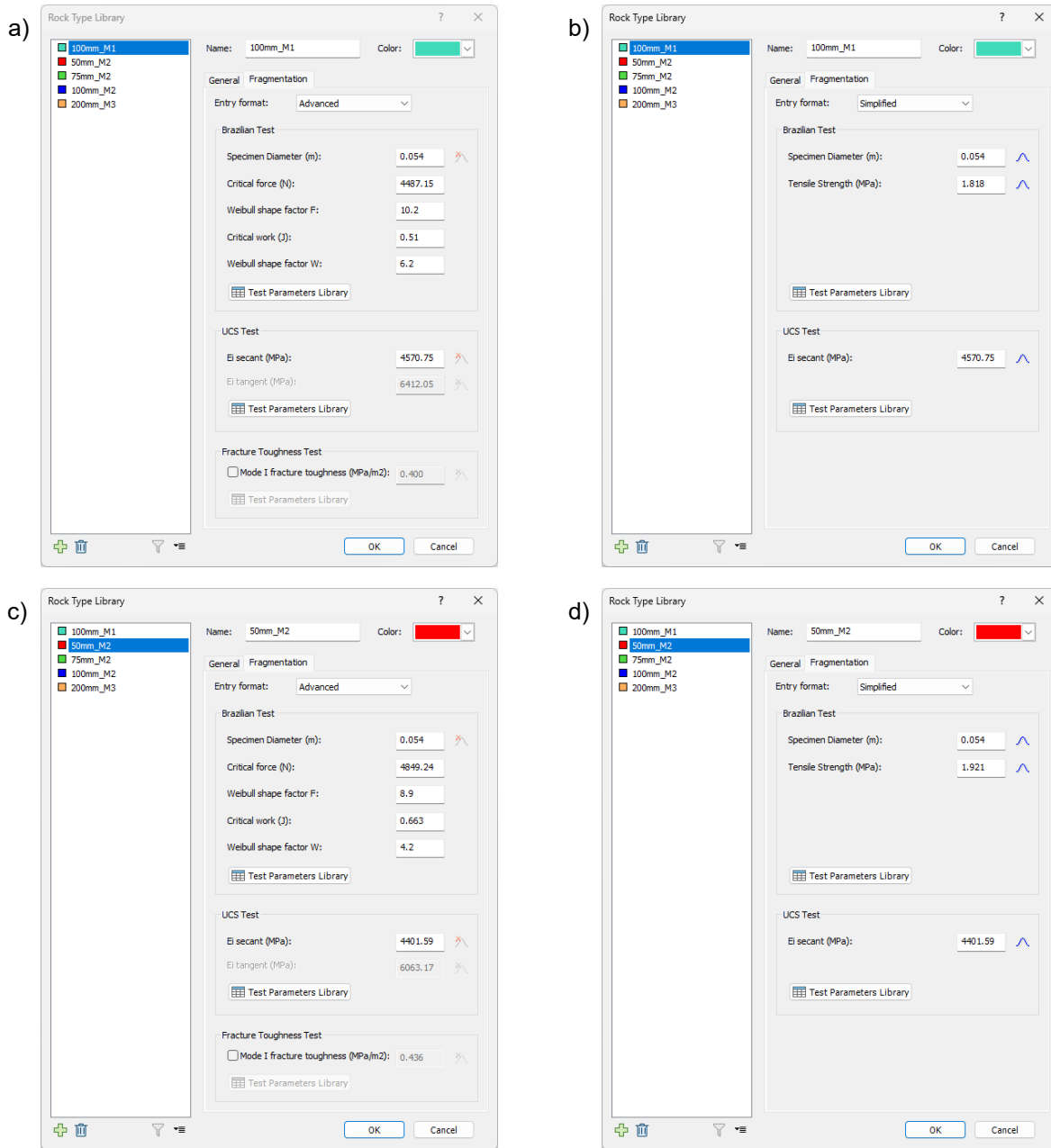


Figure 1-2 Fragmentation input parameters used for Validation Test 1. Figures a) and c) show advanced input parameters, while b) and d) show simplified inputs. Figures a) and b) refer to Material M1, whereas c) and d) refer to Material M2.

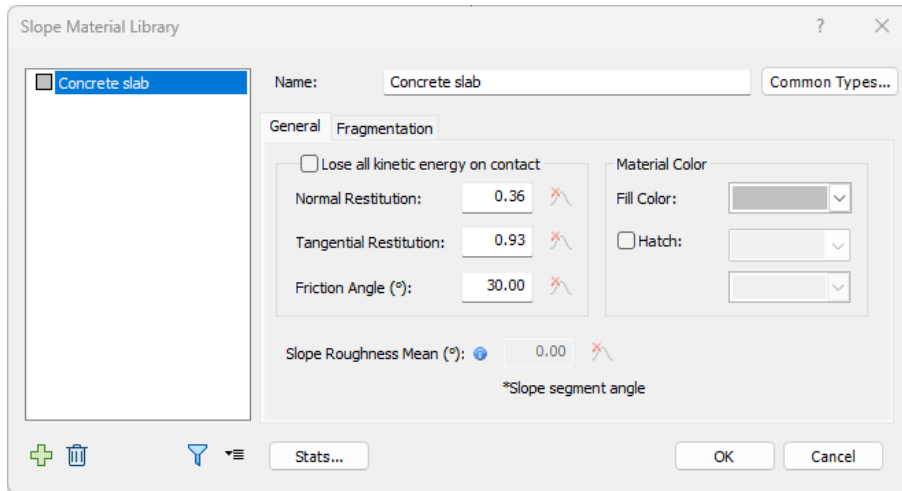


Figure 1-3 General parameters for slope used for the Validation Tests 1

Table 1-1 Drop height and equivalent impact velocity for S2 (100 mm M1).

Drop height [m]	Impact velocity [m/s]
0.898	4.20
1.156	4.76
1.191	4.83
1.275	5.00
1.542	5.50
1.660	5.71
1.836	6.00
1.939	6.17

Table 1-2 Drop height and equivalent impact velocity for S3 (50 mm M2).

Drop height [m]	Impact velocity [m/s]
1.516	5.45
1.902	6.11
2.154	6.50
2.498	7.00
2.780	7.38
2.868	7.50
3.263	8.00
3.684	8.50
3.762	8.59

Table 1-3 Drop height and equivalent impact velocity for S3 (75 mm M2).

Drop height [m]	Impact velocity [m/s]
1.180	4.81
1.459	5.35
1.542	5.50
1.836	6.00
2.154	6.50
2.498	7.00
2.868	7.50

Table 1-4 Drop height and equivalent impact velocity for S3 (100 mm M2).

Drop height [m]	Impact velocity [m/s]
0.988	4.40
1.209	4.87
1.275	5.00
1.542	5.50
1.836	6.00
2.154	6.50
2.378	6.83
2.498	7.00

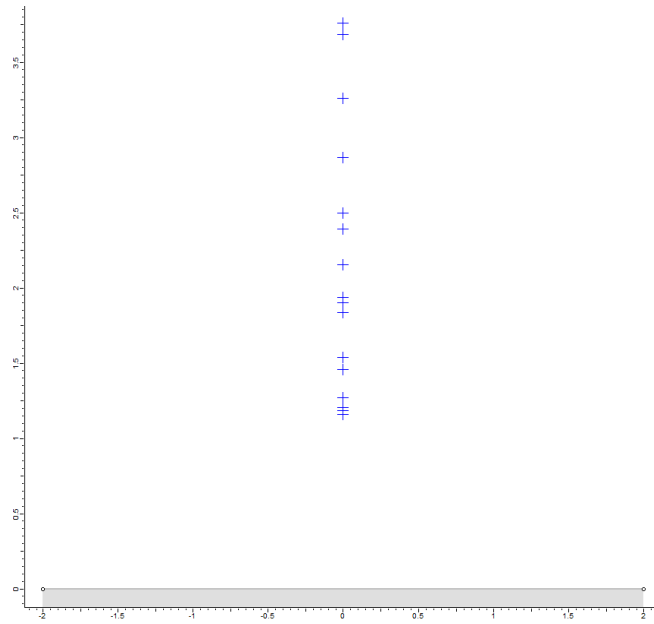


Figure 1-4 Profile and Seeder used for the Validation of Fragmentation Survival Probability.

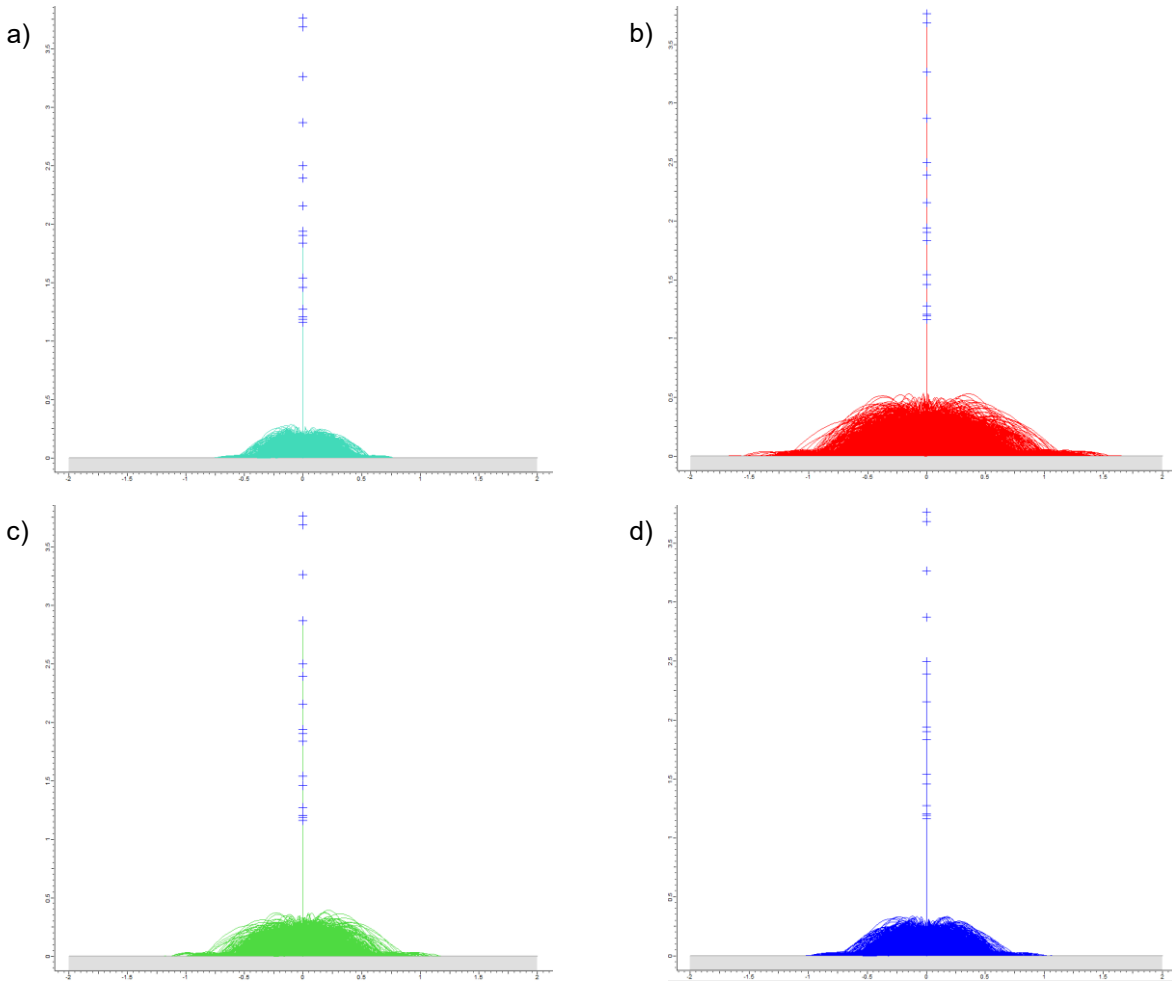


Figure 1-5 Simulation results for the Validation Tests 1.1 - Fragmentation Survival Probability. Figure a) S2 (100 mm M1), b) S3 (50 mm M2), c) S4 (75 mm M2) and d) S5 (100 mm M2).

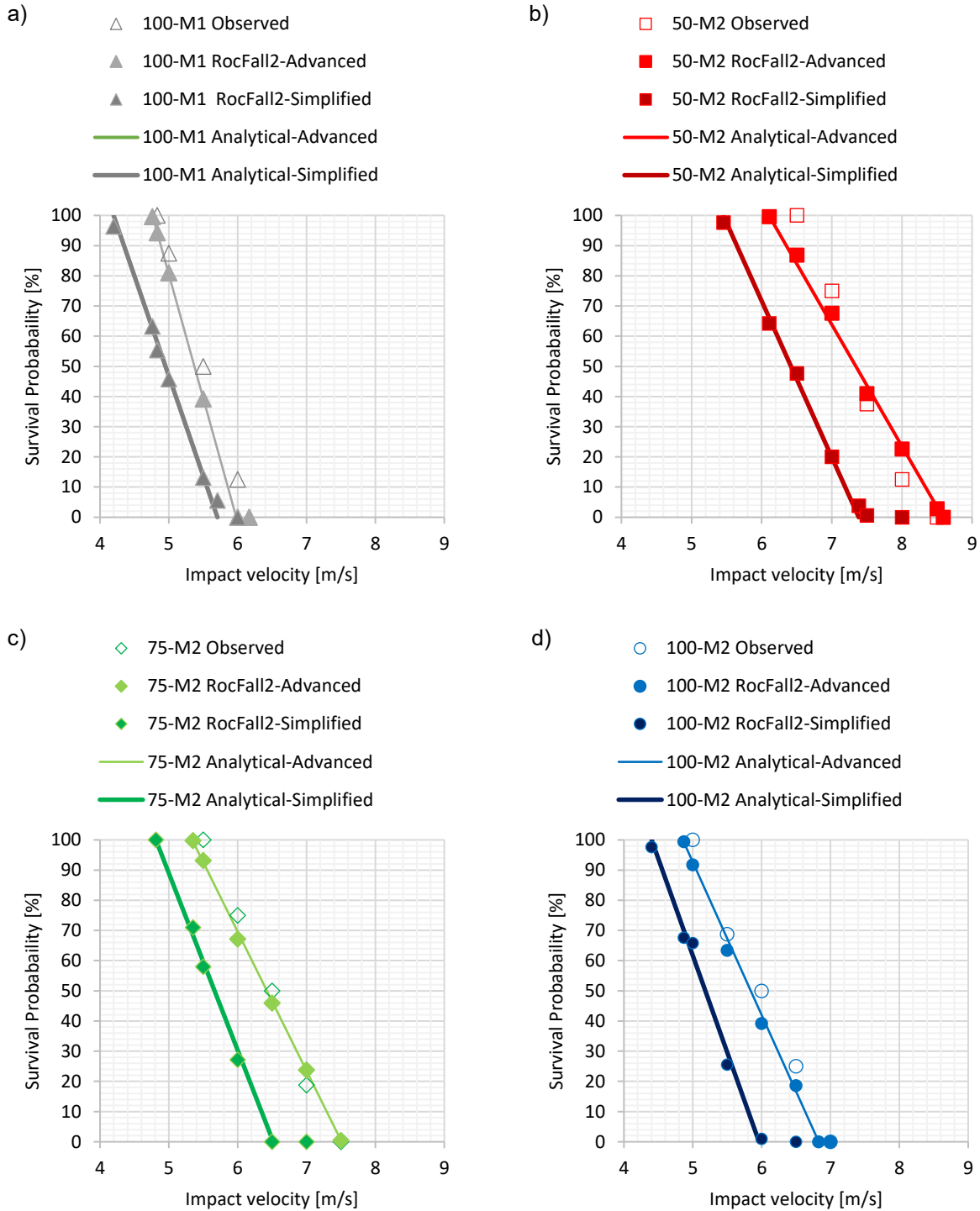


Figure 1-6 Validation of the survival probability expressed in terms of impact velocity for the experimental observations (Guccione et al. 2021a) and the simulated drop tests. The legend is referring to block diameter [mm] – material for a) 100 mm M1, b) 50 mm M2, c) 75 mm M2 and d) S4 100 mm M2. For the experimental drop tests (empty symbols), each point represents 16 drop tests while, for the simulated drops (full symbols) each point represents 500 tests. The lines represent the analytical prediction using the advanced and the simplified input parameters.

## 1.2. Validation of the mass, velocity and launch angle of the fragments

Drop test series using materials M2 and M3 and four sphere diameters (50, 75, 100, and 200 mm) were simulated, corresponding to Series S3, S4, S5, and S6 from Guccione et al. (2023), to validate the mass, velocity and launch angle of the fragments. In the experimental tests, fragment velocities were tracked in 4 out of 16 drops for each impact velocity in Series S3, S4, and S5, and in 3 drops for Series S6 (see Table 1-5). For the simulated tests, 100 blocks were dropped at each impact velocity, and an equivalent number of tests (4 for S3, S4, and S5; 3 for S6) were randomly selected for comparison. The profile and seeders used for the validation of fragmentation survival probability are illustrated in Figure 1-7.

Material M2 is the same as used in Validation 1.1; therefore, refer to Figure 1-1 and Figure 1-2 for general and advanced fragmentation inputs parameters applied for the Series S3 50 mm M2, S4 50 mm M2, and S5 100 mm M2. The general and advance fragmentation inputs parameters for material M3 are provided in Figure 1-8. As per Validation 1.1, the “Lower block mass threshold” was set to 0.001 kg and the parameters of the concrete slab are reported in Figure 1-3.

Figure 1-9 illustrates the simulation results, in term of trajectories, for the validation of the fragmentation survival probability for the four series: a) 50 mm M2, b) 75 mm M2, c) 100 mm M2 and d) 200 mm M3.

Figure 1-10 illustrates the fragment velocity normalized by the impact velocity ( $\bar{v}_f^n$ ) as a function of fragment mass across all test series. The subfigures present the experimental and simulation results from Rocfall2 for the following series: a) 50 mm M2, b) 75 mm M2, c) 100 mm M2, and d) 200 mm M3. Each data point represents an individual fragment.

Figure 1-11 shows the launch angle, defined as the ratio between the vertical and tangential components of fragment velocity ( $v_f^n$  over  $v_f^t$ ), plotted against the normalized impact velocity ( $\bar{v}_{imp}^n$ ) for all test series. Subfigure Figure 1-11a presents the experimental results, while subfigure Figure 1-11b displays the corresponding simulation outcomes from RocFall2. The variability of launch angles across different normalized impact velocities is well captured in all series. Note that, due to the 2D projection of the 3D fragment trajectories in RocFall2, the upper bound of the launch angle in the simulations is expected to be higher than in the experimental data.

Experimental data were used to define trends, and a stochastic approach was applied to select values, resulting in a satisfactory distribution of fragmentation outcomes.

Table 1-5 Tests used for validation of mass, velocity and launch angle of the fragments

Series	Diameter, Material	Range of $v_{imp}$ [m/s] tested	Total number of dropped for each $v_{imp}$		Number of tests analysed per $v_{imp}$
			Laboratory	Simulation	
S3	50 mm M2	7, 7.5, 8, 8.5	16	100	4
S4	75 mm M2	6, 6.5, 7, 7.5	16	100	4
S5	100 mm M2	5.5, 6, 6.5, 7	16	100	4
S6	200 mm M3	4, 5, 6, 7	3	100	3

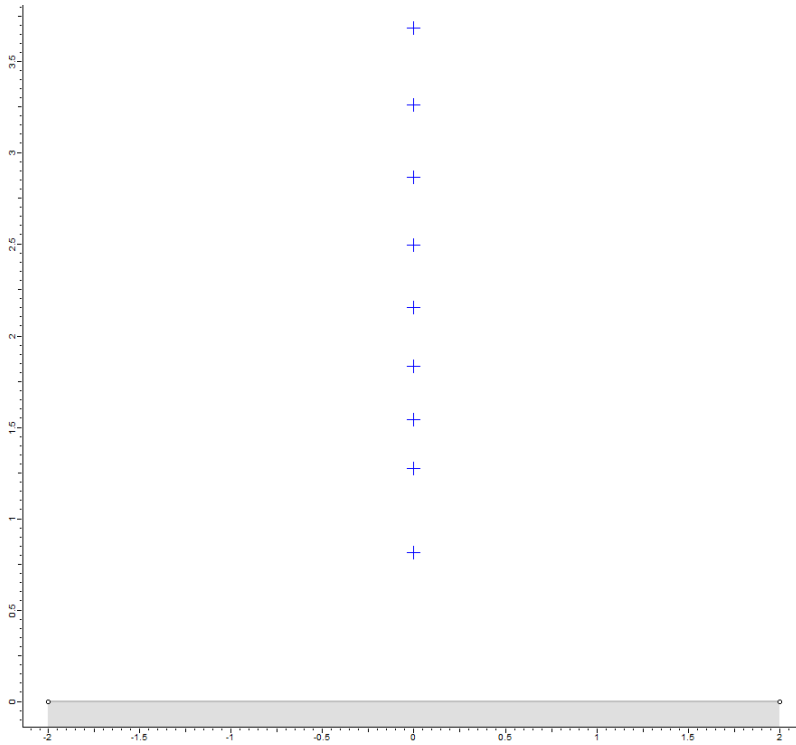


Figure 1-7 Profile and Seeder used for the validation of the mass, velocity and launch angle of the fragments.

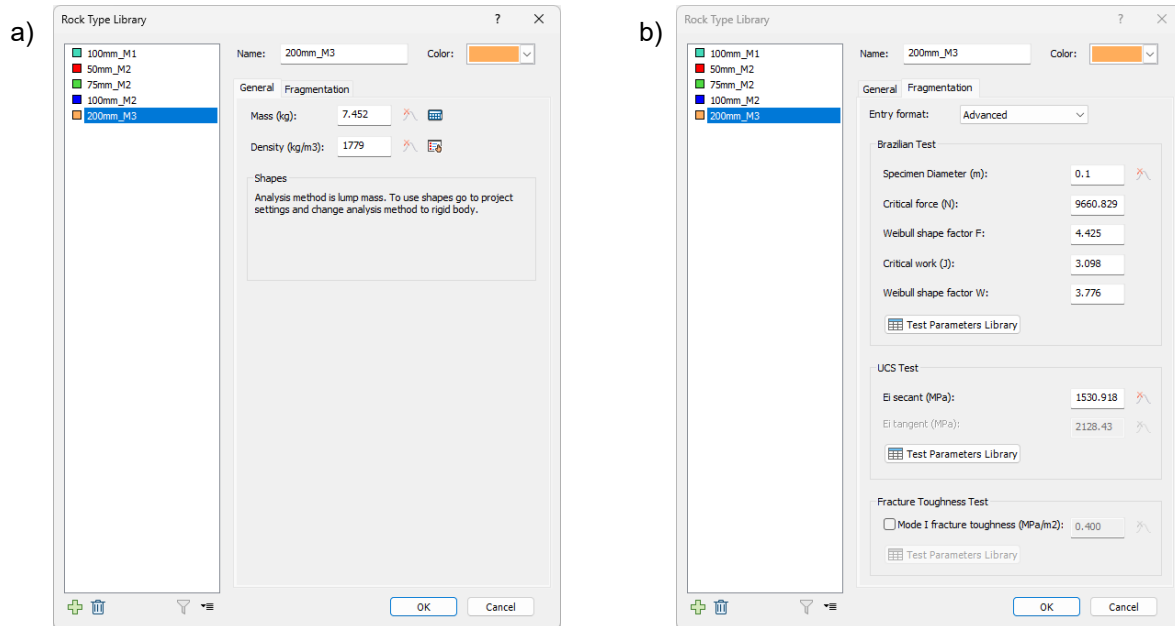


Figure 1-8 General a) and Fragmentation b) parameters used for Material M3.

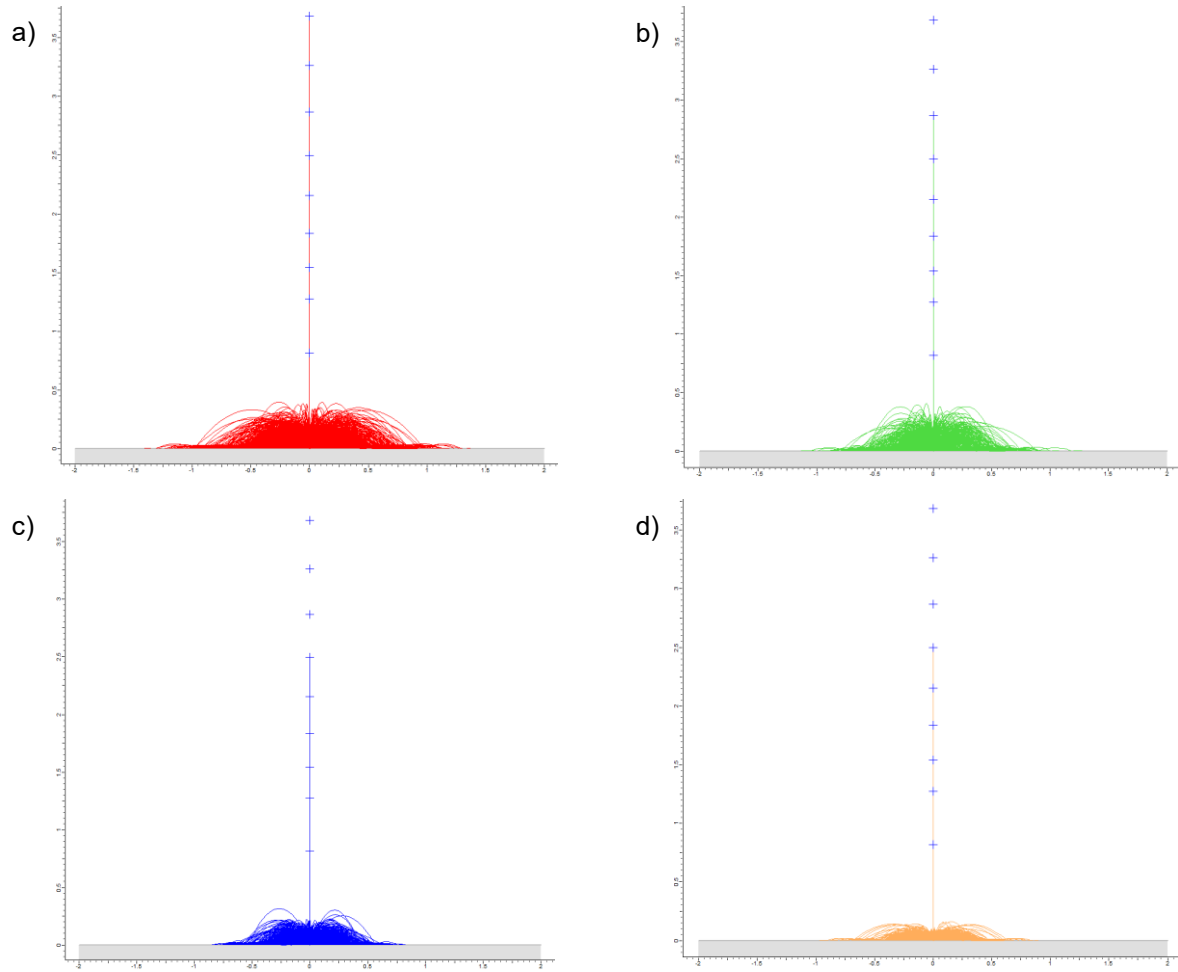


Figure 1-9 Simulation results from RocFall2 for the validation of mass, velocities and launch angle of the fragments. Figure a) S3 (50 mm M2), b) S4 (75 mm M2), c) S5 (100 mm M2) and d) S6 (200 mm M3).

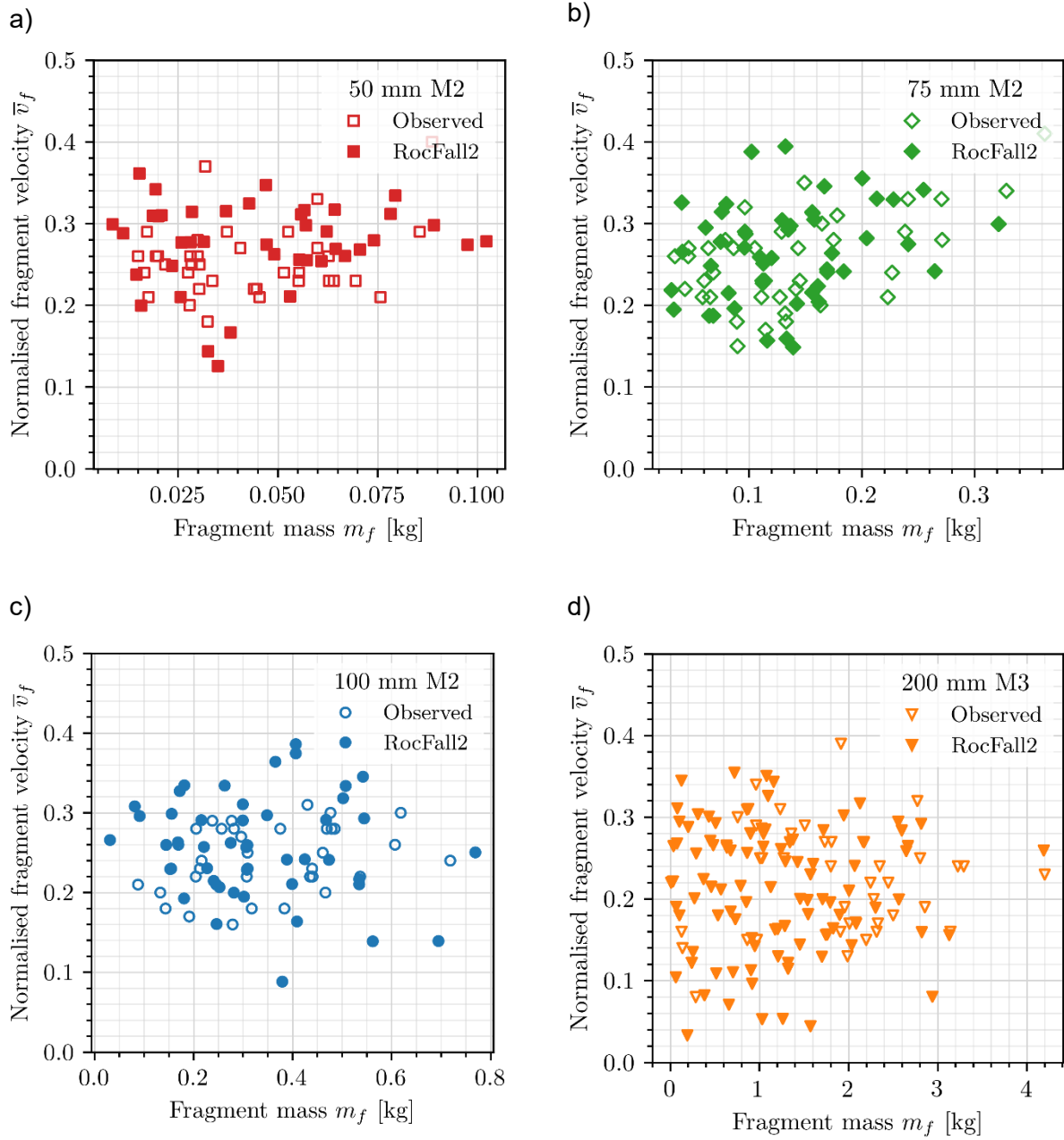


Figure 1-10 Comparison between the mass vs velocities of the fragments normalised by the impact velocity ( $\bar{v}_f$ ) observed experimentally (Guccione et al. 2023) and predicted from the simulations. Figure a) S3 (50 mm M2), b) S4 (75 mm M2), c) S5 (100 mm M2) and d) S6 (200 mm M3)

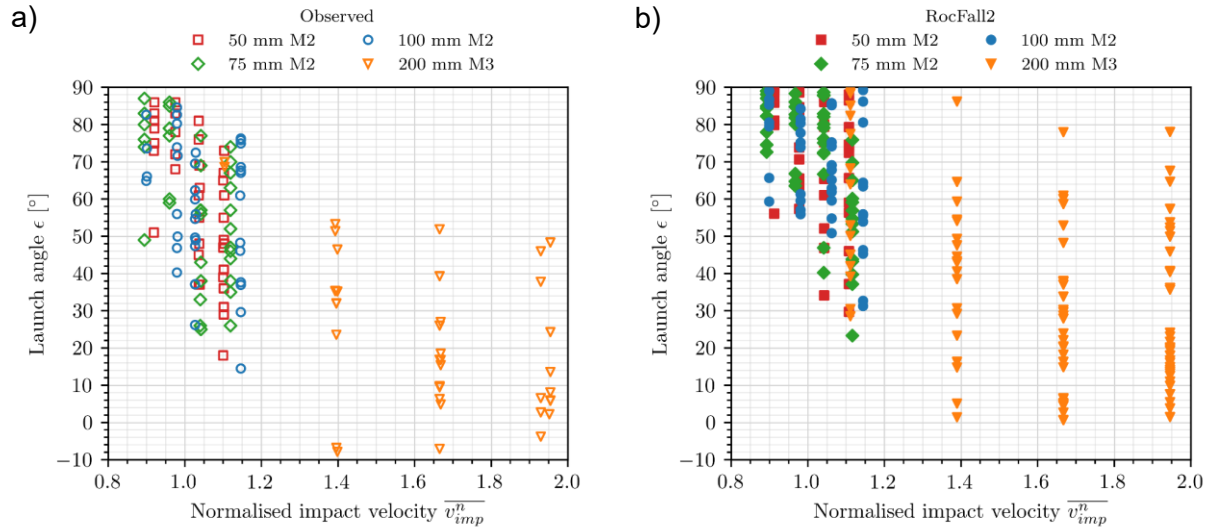


Figure 1-11 Validation of the launch angle (ratio between  $v_f^n$  over  $v_f^t$ ) as function of the normalised impact velocity ( $\bar{v}_{imp}^n$ ). a) experimental observations (Guccione et al. 2023) vs b) RocFall2 results.

## 2. Multi impact simulations

[RocFall2 Build 8.027]

A synthetic slope profile (Figure 2-1) was used to validate and show the cumulative damage effects from multiple impacts in rockfall simulations. Consistent with previous tests, material M2 (Figure 1-2c) was assigned to blocks of 100 mm diameter (Figure 1-1d), while the slope was modeled using concrete properties (Figure 1-3). Based on these parameters, the survival velocity ( $v_{surv(D)}$ ), critical velocity ( $v_{crit(D)}$ ), and fragmentation velocity ( $v_{frag(D)}$ ) were determined to be 4.85 m/s, 6.10 m/s, and 6.83 m/s, respectively. For this investigation, the coefficients of restitution were fixed: the normal coefficient ( $Rn$ ) was 0.36 and the tangential coefficient ( $Rt$ ) was 0.93. Simple geometric analysis shows that the outbound velocity is perfectly horizontal when the surface angle satisfies  $\tan \beta_s = \sqrt{Rn/Rt}$ . With the restitution values used here, the resulting angle is  $31.85^\circ$  (see Figure 2-1). Two simulation tests were compared against the analytical solution for the probability of surviving two subsequent impacts ( $SP_{(2)}$ ). This solution was obtained by combining the expression of the survival probably  $SP$  (Eq. 11 in Guccione et al. 2025) with the expression of the damage parameter  $\psi$  (Eq. 52 in Guccione et al. 2025):

$$(2-1) \quad SP_{(2)} = \left( 1 - \bar{v}_{imp(2)}^n \sqrt{\frac{1 + \frac{1}{m_v} - 0.36}{1 + \frac{1}{m_v} - \bar{v}_{imp(1)}^n}} \right) \frac{m_v}{e} + 0.37$$

where  $\bar{v}_{imp(1)}^n$  and  $\bar{v}_{imp(2)}^n$  are the normalized impact velocity of the first and second impact, respectively. The parameter  $m_v$  is Weibull shape parameter associated to the survival probability for impacting block, expressed in terms of impact velocity. This parameter is calculated for the input parameter, see Section 3.2 of Guccione et al. (2025) for further details.

The two simulation tests can be summarized as follows:

1.  $h_1$  fixed while  $h_2$  variable. (Figure 2-1a) Blocks were dropped from a fixed height ( $h_1$ ) corresponding to a normalized impact velocity ( $\bar{v}_{imp(1)}^n$ ) equal to the survival velocity ( $v_{surv(D)}$ ) normalized by the critical velocity ( $v_{crit(D)}$ ), resulting in  $\bar{v}_{imp(1)}^n = 0.8$  for the material used in this analysis. In contrast, the height of the second impact ( $h_2$ ) was varied to produce normalized impact velocities ( $\bar{v}_{imp(2)}^n$ ) ranging from 0.36 to  $1+1/m_v$  (see Fig. 13 in Guccione et al. 2025). A total of 13 different values of  $\bar{v}_{imp(2)}^n$  were tested within this range (see equivalent profiles and seeders coordinates in Table 2-1), with 500 blocks dropped for each test case.
2.  $h_1$  variable while  $h_2$  fixed. (Figure 2-1b) Blocks were dropped from varying heights ( $h_1$ ) corresponding to normalized impact velocities  $\bar{v}_{imp(1)}^n$  ranging from 0.36 to  $1+1/m_v$ , while the second impact height ( $h_2$ ) was kept constant, yielding a normalized impact velocity  $\bar{v}_{imp(2)}^n = 0.8$ , equivalent to the survival velocity  $v_{surv(D)}$ . For this analysis, using the “Point Seeder Series” a total of 12 Seeders of  $\bar{v}_{imp(1)}^n$  were tested across the specified range (see Table 2-2), with 500 blocks dropped for each test case.

As per Validation 1, the “Lower block mass threshold” was set to 0.001 kg.

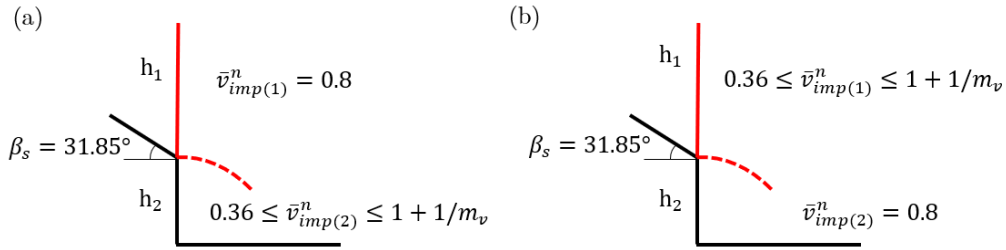


Figure 2-1 Profile and normalized impact velocities ( $\bar{v}_{imp(1)}^n$  and  $\bar{v}_{imp(2)}^n$ ) used in the multi-impact simulations: (a) Analysis 1 ( $h_1$  fixed while  $h_2$  variable) and (b) Analysis 2 ( $h_1$  variable while  $h_2$  fixed).  $h_1$  represents the drop height corresponding to the normalized impact velocity  $\bar{v}_{imp(1)}^n$ , while  $h_2$  corresponds to the second impact height, associated with  $\bar{v}_{imp(2)}^n$ .  $\beta_s$  denotes the slope angle.

Profile 1		Profile 2		Profile 3		Profile 4		Profile 5	
X [m]	Y [m]								
-2.000	1.488	-2.000	1.603	-2.000	1.718	-2.000	1.833	-2.000	1.947
0.000	0.246	0.000	0.361	0.000	0.475	0.000	0.590	0.000	0.705
0.000	0.000	0.000	0.000	0.000	0.000	0.000	0.000	0.000	0.000
6.000	0.000	6.000	0.000	6.000	0.000	6.000	0.000	6.000	0.000
Seeder 1		Seeder 2		Seeder 3		Seeder 4		Seeder 5	
X [m]	Y [m]								
-0.001	1.913	-0.001	2.027	-0.001	2.142	-0.001	2.257	-0.001	2.371

Profile 6		Profile 7		Profile 8		Profile 9		Profile 10	
X [m]	Y [m]	X [m]	Y [m]						
-2.000	2.062	-2.000	2.177	-2.000	2.291	-2.000	2.550	-2.000	2.808
0.000	0.820	0.000	0.934	0.000	1.049	0.000	1.307	0.000	1.565
0.000	0.000	0.000	0.000	0.000	0.000	0.000	0.000	0.000	0.000
6.000	0.000	6.000	0.000	6.000	0.000	6.000	0.000	6.000	0.000
Seeder 6		Seeder 7		Seeder 8		Seeder 9		Seeder 10	
X [m]	Y [m]	X [m]	Y [m]						
-0.001	2.486	-0.001	2.601	-0.001	2.716	-0.001	2.974	-0.001	3.232

Profile 11		Profile 12		Profile 13	
X [m]	Y [m]	X [m]	Y [m]	X [m]	Y [m]
-2.000	3.066	-2.000	3.324	-2.000	3.582
0.000	1.823	0.000	2.082	0.000	2.340
0.000	0.000	0.000	0.000	0.000	0.000
6.000	0.000	6.000	0.000	6.000	0.000
Seeder 11		Seeder 12		Seeder 13	
X [m]	Y [m]	X [m]	Y [m]	X [m]	Y [m]
-0.001	3.490	-0.001	3.748	0.999	4.006

Table 2-1 Profiles and Seeders used for Validation Test 2.1 ( $h_1$  fixed while  $h_2$  variable).

Table 2-2 Profile and Point Seeder Series used for Validation Test 2.2 (h<sub>1</sub> variable while h<sub>2</sub> fixed).

Profile		Point Seeder Series					
X [m]	Y [m]		X [m]	Y [m]	Angle (deg)	Interval [m]	Count
-2.000	2.445	from	-0.001	1.500	90	0.25	12
0.000	1.203	to	-0.001	4.500			
0.000	0.000						
6.000	0.000						

## 2.1. Influence of Severity of the Second Impact (h<sub>1</sub> fixed while h<sub>2</sub> variable) on the Survival Probability of the Second Impact

In the first multi-impact simulation analysis, blocks were dropped from a height h<sub>1</sub>, corresponding to the normalized survival velocity  $v_{surv(D)}$ , which equals 0.8 in this case. The height of the second impact (h<sub>2</sub>) was varied to produce normalized impact velocities  $\bar{v}_{imp(2)}^n$  ranging from 0.36 to  $1+1/m_v$  (see Figure 2-1 and Table 2-1). Six out of the 13 Profiles used for the Validation 2.1, are shown in Figure 2-2.

Figure 2-3 shows selected trajectory examples from the first multi-impact simulation analysis, where the second impact height (h<sub>2</sub>) was varied. Specifically, the subfigures illustrate results for six different profiles (a) Profile 2, b) Profile 4, c) Profile 6, d) Profile 8, e) Profile 10, f) Profile 12) with an equivalent normalized impact velocities at the second impact ( $\bar{v}_{imp(2)}^n$ ) corresponding to: a) 0.44, b) 0.56, c) 0.66, d) 0.74, e) 0.91, and f) 1.06. Note that, due to the fixed values of  $R_n$  and  $R_t$ , all intact blocks follow identical trajectories.

Figure 2-4 illustrates the survival probability for the second impact ( $SP_{(2)}$ ), comparing both simulated results from RocFall2 and analytical solutions that account for damage, as well as the analytical solution without considering damage. Since all blocks experience a first impact at a normalized velocity  $\bar{v}_{imp(1)}^n$  equal to the survival velocity  $v_{surv(D)}$ , none of them break during the initial impact.

If damage from the first impact is ignored, all blocks will survive the second impact as long as the normalized impact velocity  $\bar{v}_{imp(2)}^n$  remains below the survival threshold  $v_{surv(D)}$ . For values of  $\bar{v}_{imp(2)}^n$  greater than 0.8, the survival probability  $SP_{(2)}$  decreases linearly with increasing impact velocity until it reaches  $1+1/m_v$  (equal to 1.12 in this case), corresponding to the fragmentation velocity  $v_{frag(D)}$ .

When damage from the first impact is considered, blocks will survive the second impact only if  $\bar{v}_{imp(2)}^n < 0.52$ . For higher velocities, the probability of fragmentation increases, reaching zero survival probability at  $\bar{v}_{imp(2)}^n > 0.73$ . As shown in Figure 2-4, the numerical (from RocFall2) and analytical solutions are in good agreement, highlighting how damage from the first impact significantly affects the survival probability during the second impact.

Figure 2-5 reports the number of intact blocks, fragments, and the total number of blocks (i.e., the sum of intact blocks and fragments). For normalized impact velocities  $\bar{v}_{imp(2)}^n < 0.52$  the total number of blocks equals the number of intact blocks, which also corresponds to the number of simulations. For  $0.52 < \bar{v}_{imp(2)}^n < 0.73$ , the number of intact blocks decreases while the number of fragments increases, resulting in a total block count equal to the sum of both. When  $\bar{v}_{imp(2)}^n > 0.73$ , all blocks are fully fragmented, and the total number of fragments increases with impact velocity.

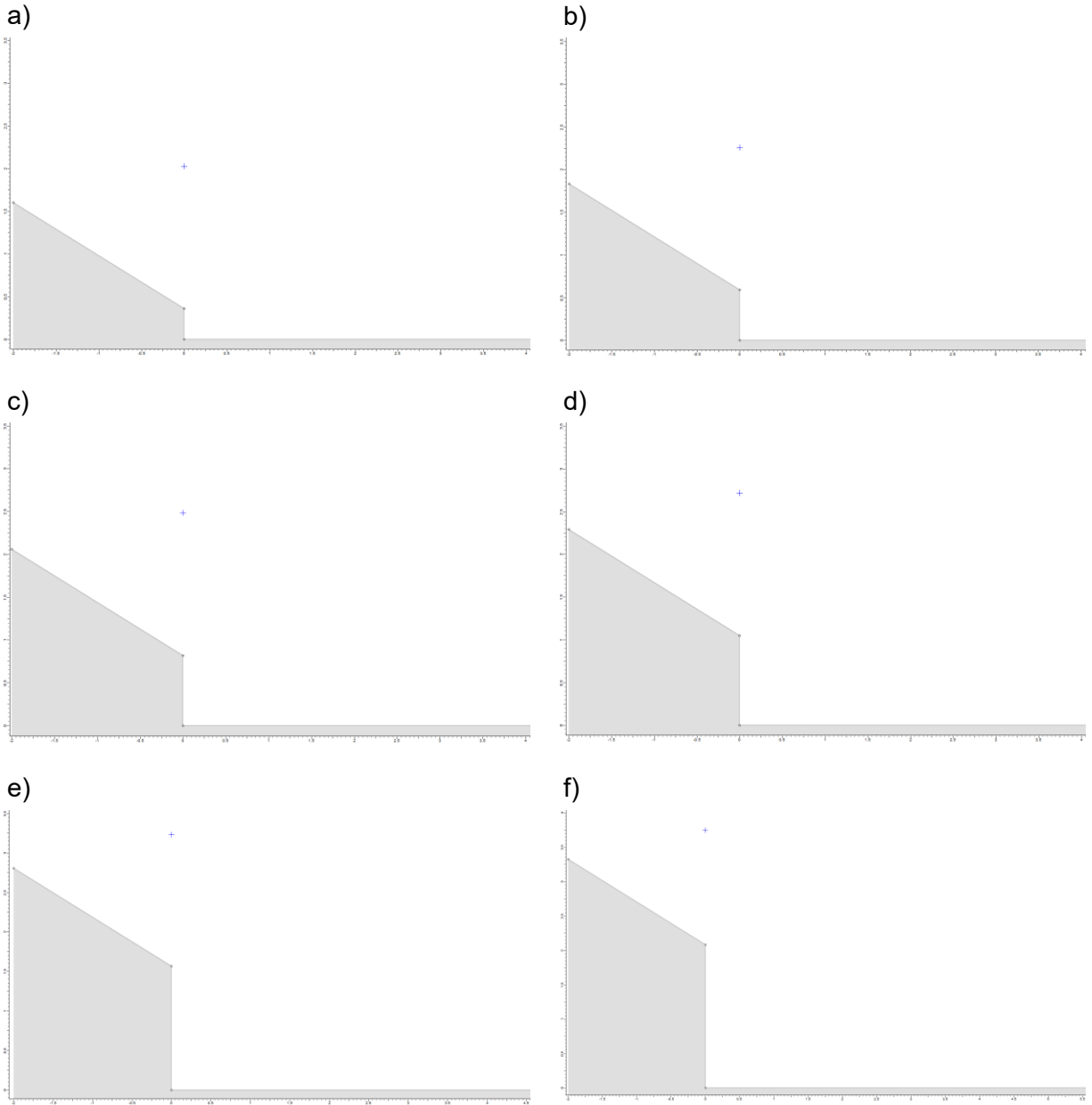


Figure 2-2 Example of Profiles and Seeders used for the multi-impact tests Validation 2.1:  $h_1$  fixed while  $h_2$  variable. The subfigures are referring to a) Profile 2 -  $\bar{v}_{imp(2)}^n = 0.44$ , b) Profile 4 -  $\bar{v}_{imp(2)}^n = 0.56$ , c) Profile 6 -  $\bar{v}_{imp(2)}^n = 0.66$ , d) Profile 8 -  $\bar{v}_{imp(2)}^n = 0.74$ , e) Profile 10 -  $\bar{v}_{imp(2)}^n = 0.91$ , f) Profile 12 -  $\bar{v}_{imp(2)}^n = 1.06$  of Table 2-2.

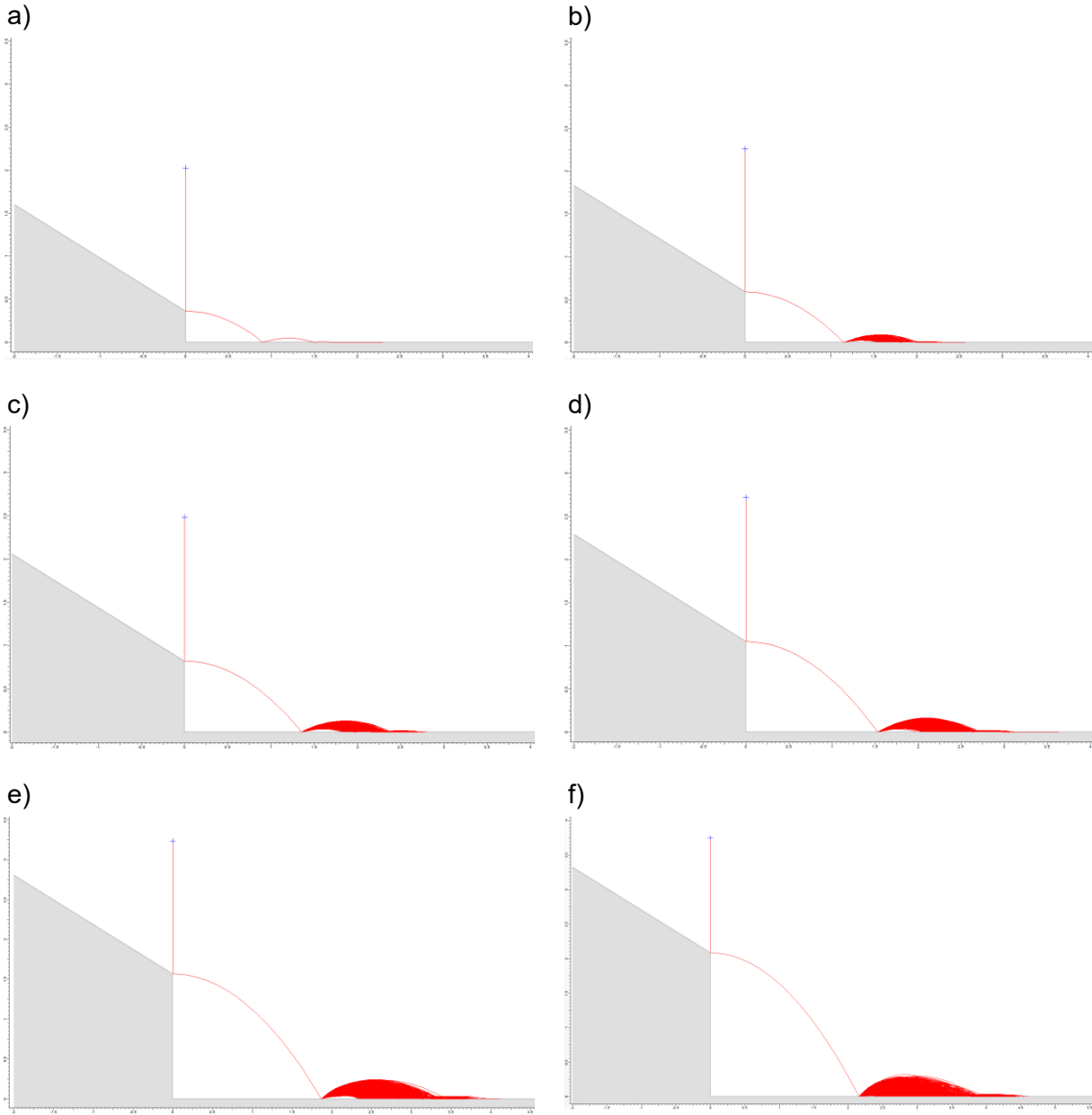


Figure 2-3 Simulation results from RocFall2 for the validation of the multi-impact tests Validation 2.1:  $h_1$  fixed while  $h_2$  variable. The subfigures are referring to results Profile 2 -  $\bar{v}_{imp(2)}^n = 0.44$ , b) Profile 4 -  $\bar{v}_{imp(2)}^n = 0.56$ , c) Profile 6 -  $\bar{v}_{imp(2)}^n = 0.66$ , d) Profile 8 -  $\bar{v}_{imp(2)}^n = 0.74$ , e) Profile 10 -  $\bar{v}_{imp(2)}^n = 0.91$ , f) Profile 12 -  $\bar{v}_{imp(2)}^n = 1.06$  (see Table 2-2).

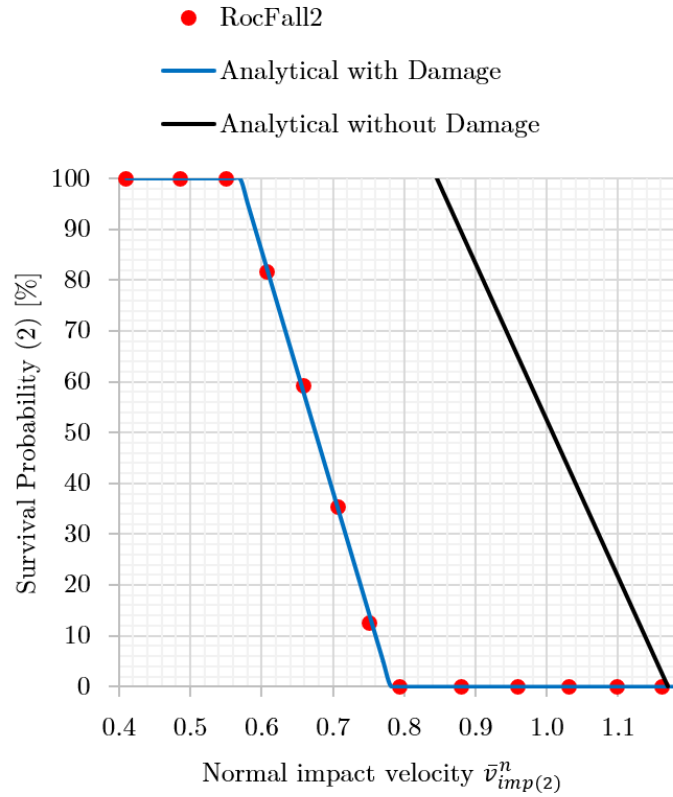


Figure 2-4 Survival probability of the second impact (2) with (numerical and analytical) and without damage module (analytical). Blocks were dropped from an equivalent normalised impact velocity  $\bar{v}_{imp(1)}^n$  equal to  $v_{surv(D)}$ , while normalised impact velocity of the second impact  $\bar{v}_{imp(2)}^n$  was varied.

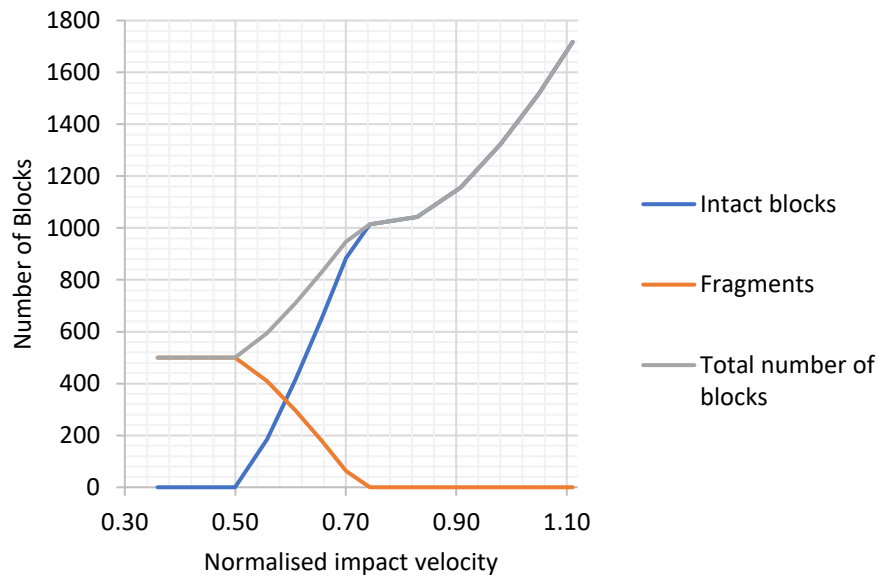


Figure 2-5 Total Number of Blocks as function of the normalised impact velocity of the second impact. Blocks were dropped from an equivalent normalised impact velocity  $\bar{v}_{imp(1)}^n$  equal to  $v_{surv(D)}$ .

## 2.2. Influence of Severity of the First Impact ( $h_1$ variable while $h_2$ fixed) on the Survival Probability of the Second Impact

In the second multi-impact simulation analysis, blocks were dropped from varying heights ( $h_1$ ), corresponding to normalized first-impact velocities ( $\bar{v}_{imp(1)}^n$ ) ranging from 0.36 to  $1+1/m_v$ . The second impact height ( $h_2$ ) was kept constant, corresponding to a normalized impact velocity ( $\bar{v}_{imp(2)}^n$ ) of 0.8, equal to the survival velocity ( $v_{surv(D)}$ ) (see Figure 2-1 and Table 2-2). Figure 2-6 illustrate Profile and 12 Seeders used for the multi-impact tests 2 (see details in Table 2-2). Figure 2-7 shows the trajectory results from the second multi-impact test, with varying  $h_1$ .

Figure 2-8 presents the survival probability for the second impact ( $SP_{(2)}$ ), comparing both numerical from RocFall2 and analytical solutions. Since the second impact velocity is equal to the survival threshold, blocks that survive the first impact—regardless of how severe—would also survive the second impact if damage is not considered. However, when damage from the first impact is accounted for, the survival probability at the second impact decreases as  $\bar{v}_{imp(1)}^n$  increases. Figure 2-8 shows that for  $\bar{v}_{imp(1)}^n > 0.36$ ,  $SP_{(2)}$  declines (non-linearly) due to increasing damage from the first impact, reaching zero at  $\bar{v}_{imp(1)}^n = 0.73$ . Note that, for  $\bar{v}_{imp(1)}^n < 0.8$ , all blocks survive the first impact, but may still fragment at the second impact due to accumulated damage. For  $\bar{v}_{imp(1)}^n > 0.8$ , some blocks fragment during the first impact, and those that survive carry damage that leads to fragmentation during the second impact under the given test conditions.

Figure 2-9 shows the number of intact blocks, fragments produced at the first and second impacts, and the total number of blocks (i.e., the sum of intact blocks and all fragments). As the normalized impact velocity increases, the severity of damage from the first impact also increases, resulting in fewer intact blocks surviving the second impact and more fragments produced at the second impact. Note that for  $\bar{v}_{imp(1)}^n < 0.8$ , all blocks survive the first impact, so no fragments are generated in this range. For  $\bar{v}_{imp(1)}^n > 0.8$ , blocks can fragment during the first impact, leading to an increase in the number of fragments from the first impact, while the number of fragments produced at the second impact decreases since fewer blocks survive the first impact.

For normalized impact velocities  $\bar{v}_{imp(2)}^n < 0.52$  the total number of blocks equals the number of intact blocks, which also corresponds to the number of simulations. For  $0.52 < \bar{v}_{imp(2)}^n < 0.73$ , the number of intact blocks decreases while the number of fragments increases, resulting in a total block count equal to the sum of both. When  $\bar{v}_{imp(2)}^n > 0.73$ , all blocks are fully fragmented, and the total number of fragments increases with impact velocity.

These results highlight the critical role of initial impact velocity in determining survival probability across multiple impacts, emphasizing the importance of accounting for cumulative damage in rockfall hazard simulations.

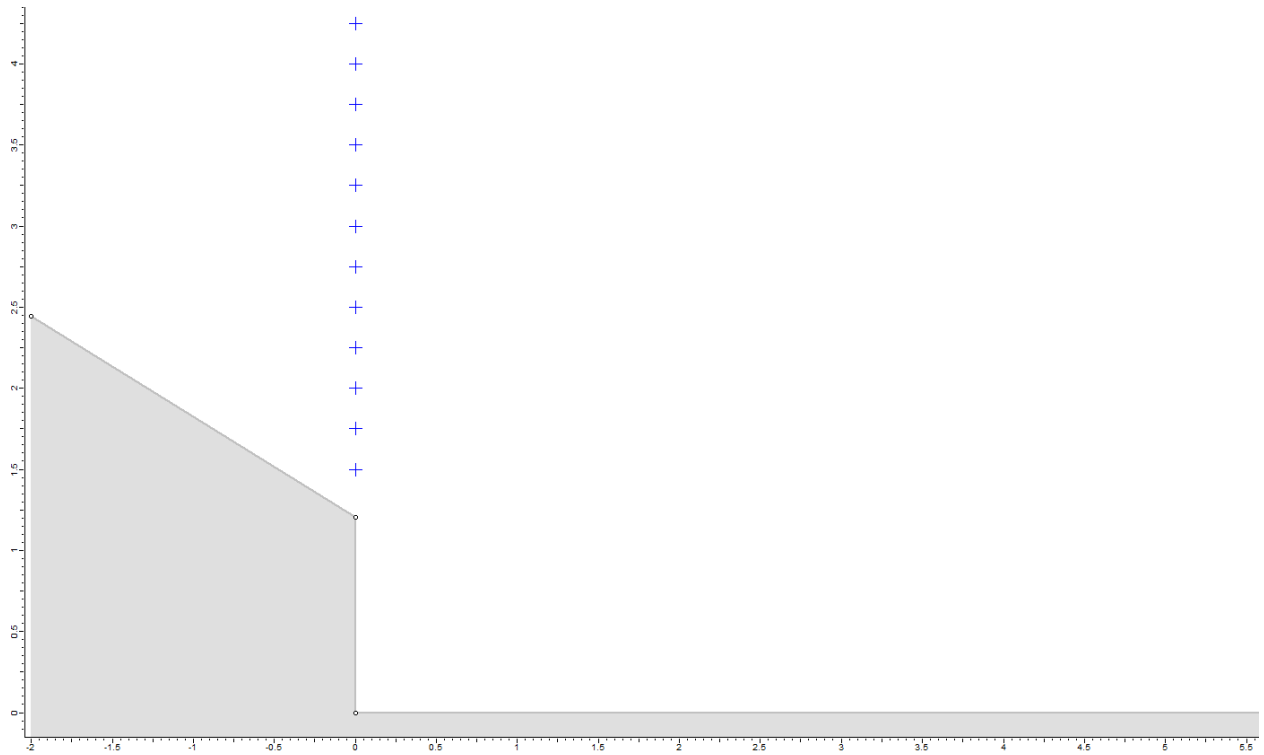


Figure 2-6 Profile and 12 Seeders used for the multi-impact tests 2:  $h_1$  variable while  $h_2$  fixed.

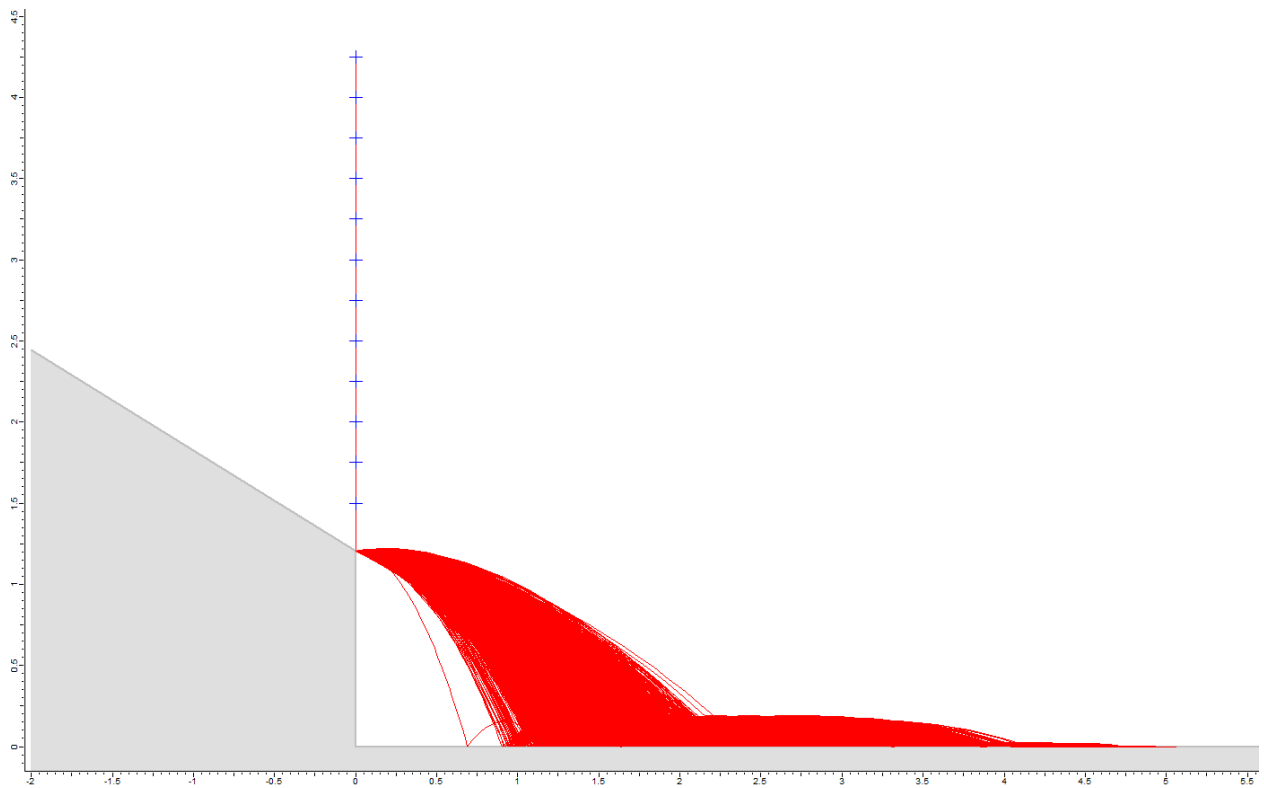


Figure 2-7 Trajectories results for the multi-impact tests 2:  $h_1$  variable while  $h_2$  fixed.

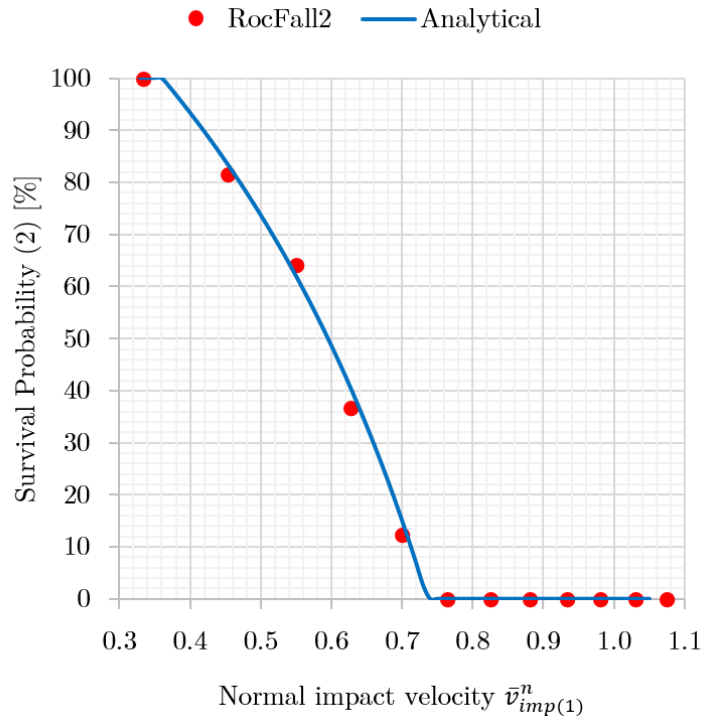


Figure 2-8 Numerical and analytical probability of surviving (SP) a second impact of an equivalent normalised impact velocity ( $\bar{v}_{imp(2)}^n$ ) of 0.8 (correspond to  $v_{surv(D)}$ ) given that block survived the first impact as a function of normalised impact velocity at first impact ( $\bar{v}_{imp(1)}^n$ ).

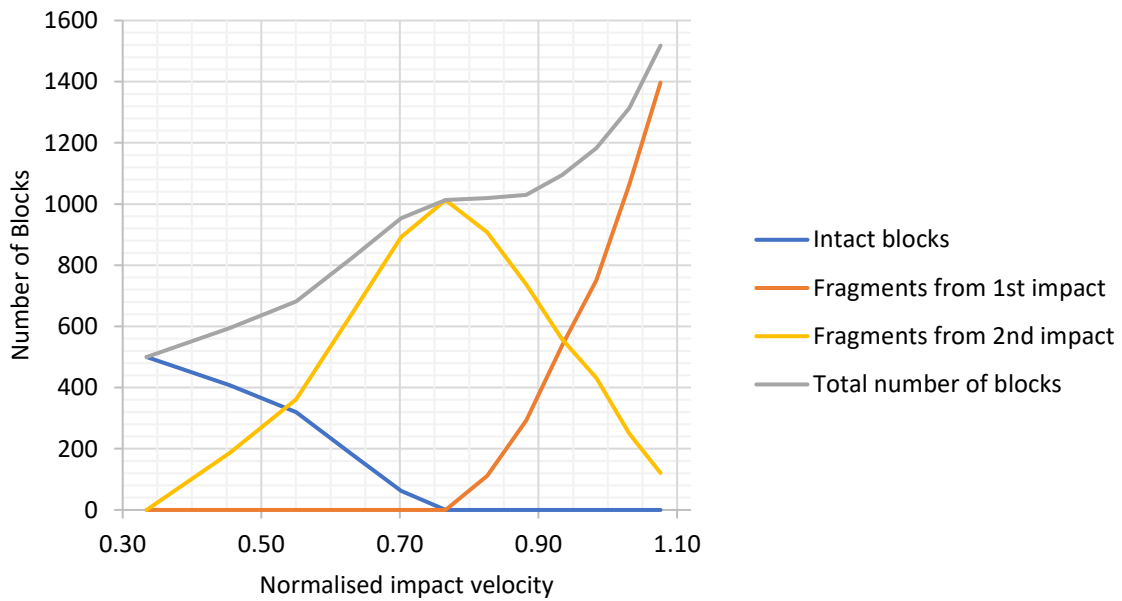


Figure 2-9 Total Number of Blocks as function of the normalised impact velocity of the first impact. The normalised impact velocity  $\bar{v}_{imp(2)}^n$  was constant and equal to  $v_{surv(D)}$ .

### 3. In-situ tests simulations

[RocFall2 Build 8.027]

For the final validation, in-situ tests conducted in Vallirana, Spain (Gili et al., 2016; 2022; Matas et al., 2020; Prades-Valls et al., 2022) were replicated and compared where possible. In particular, Test 4 from Gili et al. (2022) was selected, which involved dropping 24 limestone blocks ranging from 0.5 to 2.25 m<sup>3</sup>, with an average volume of 1 m<sup>3</sup> and a standard deviation of 0.5 m<sup>3</sup>. The blocks were released from a height of 8.5 m along a selected slope profile (see Figure 3-1).

The simplified input parameters for the fragmentation module were derived from two uniaxial compressive strength (UCS) tests and three Brazilian tensile (BT) tests (see Figure 3-2) reported in Gili et al. (2022). Although this number of tests is insufficient to fully capture the material variability (as noted by Guccione et al., 2022), the limited availability of in-situ fragmentation-focused experiments makes this dataset valuable for model validation. It is also important to note that the natural blocks used in the field tests were not spherical and may have contained defects or microcracks, potentially influencing the fragmentation outcomes.

To account for this, 24 blocks were initially simulated, and the Young's modulus of the slope was calibrated to match the observed number of fragments (approximately 250 for fragments with mass > 0.01 kg; see Figure 7 in Matas et al., 2020). As a result of this calibration, the Young's modulus was set to 0.4 GPa, which produced 242 fragments (with mass > 0.01 kg).

The coefficients of restitution and friction angles used in the simulations are reported in Table 3. The coefficient of restitution values for limestone (Lt) were taken from Table 2 of Prades-Valls et al. (2022), while the coefficient of restitution and friction angle for the toe of the slope (Talus) were calibrated to match the runout observed in the unfragmented field tests.

Zero initial velocities were imposed in the simulations. The scaling of the normal coefficient of restitution and rotational velocity were not considered. A lower block mass threshold of 0.01 kg was applied.

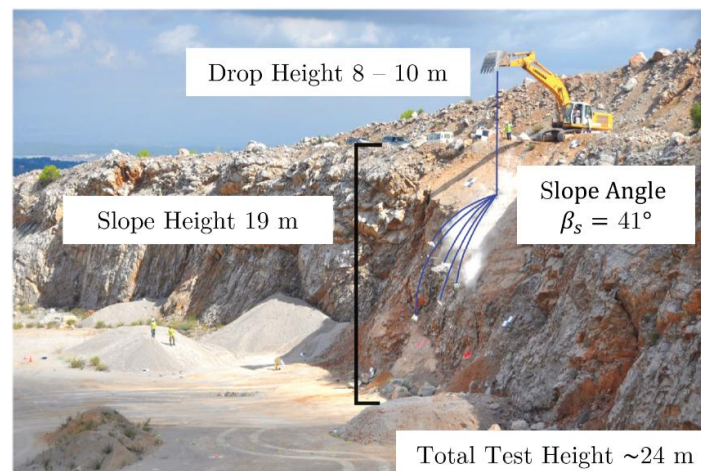


Figure 3-1. Overview of the full slope upon which the tests were performed (modified after Matas et al. (2020)).

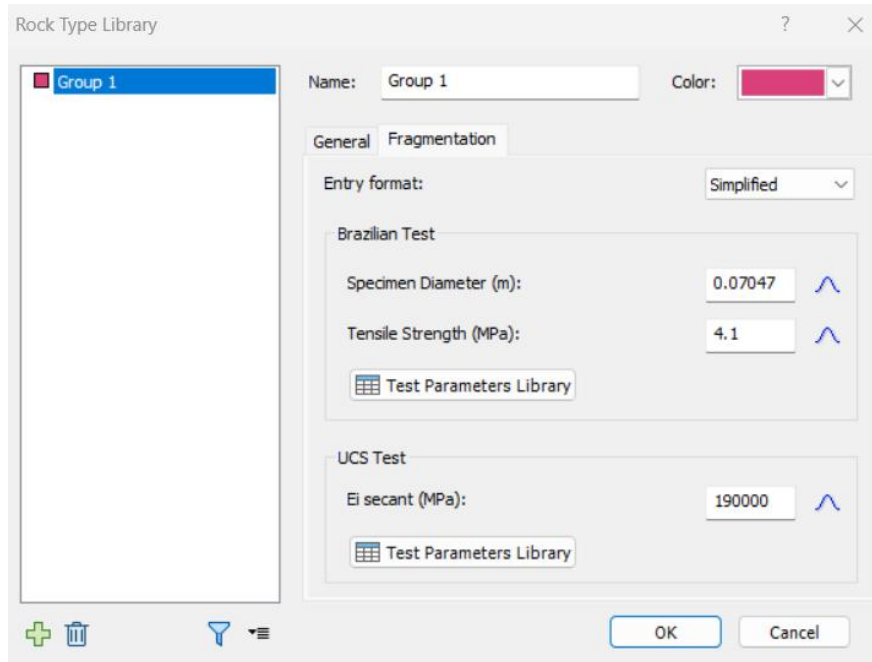


Figure 3-2. Input parameters of the rock type.

Table 3. Coefficient of restitutions and friction angles used for the simulations of the in-situ tests.

	Mean		Std		Min		Max	
	<i>Ls</i>	<i>Talus</i>	<i>Ls</i>	<i>Talus</i>	<i>Ls</i>	<i>Talus</i>	<i>Ls</i>	<i>Talus</i>
$CoR^n$	0.24	0.40*	0.11	0.04*	0.12	0.28*	0.37	0.52*
$CoR^t$	0.56	0.80*	0.06	0.04*	0.64	0.68*	0.49	0.92*
$\phi$ [°]	20*	30*	3*	3*	15*	25*	25*	35*
* assumed value								

For the final validation, a comparison was made between 100 simulated blocks—with and without fragmentation. The results of these simulations in term trajectories, endpoint location and total kinetic energy are shown in Figure 3-3, Figure 3-4 and Figure 3-5, respectively.

Figure 3-4 indicates that the endpoint locations for the two simulations (unfragmented and fragmented) are similar. However, a major difference lies in the number of blocks: the simulation with fragmentation produced a total of 1,015 fragments generated during multiple impacts on the slope (see Figure 3-4b).

This fragmentation significantly affects the kinetic energy at the toe of the slope. Comparing the two subfigures in Figure 3-5, the maximum total kinetic energy (at approximately  $x = 9\text{m}$ ) decreases from 730 kJ (unfragmented) to 342 kJ (fragmented), representing a reduction of more than 50%. The 90th percentile drops from 473 kJ to 123 kJ, a reduction of 74%. At  $x \approx 15\text{m}$ , this reduction increases to about 80% for the maximum value and 92% for the 90th percentile.

This substantial reduction in kinetic energy results from the fragmentation process, which can significantly influence the design of protection structures and underscores the importance of accounting for block fragmentation in rockfall simulations.

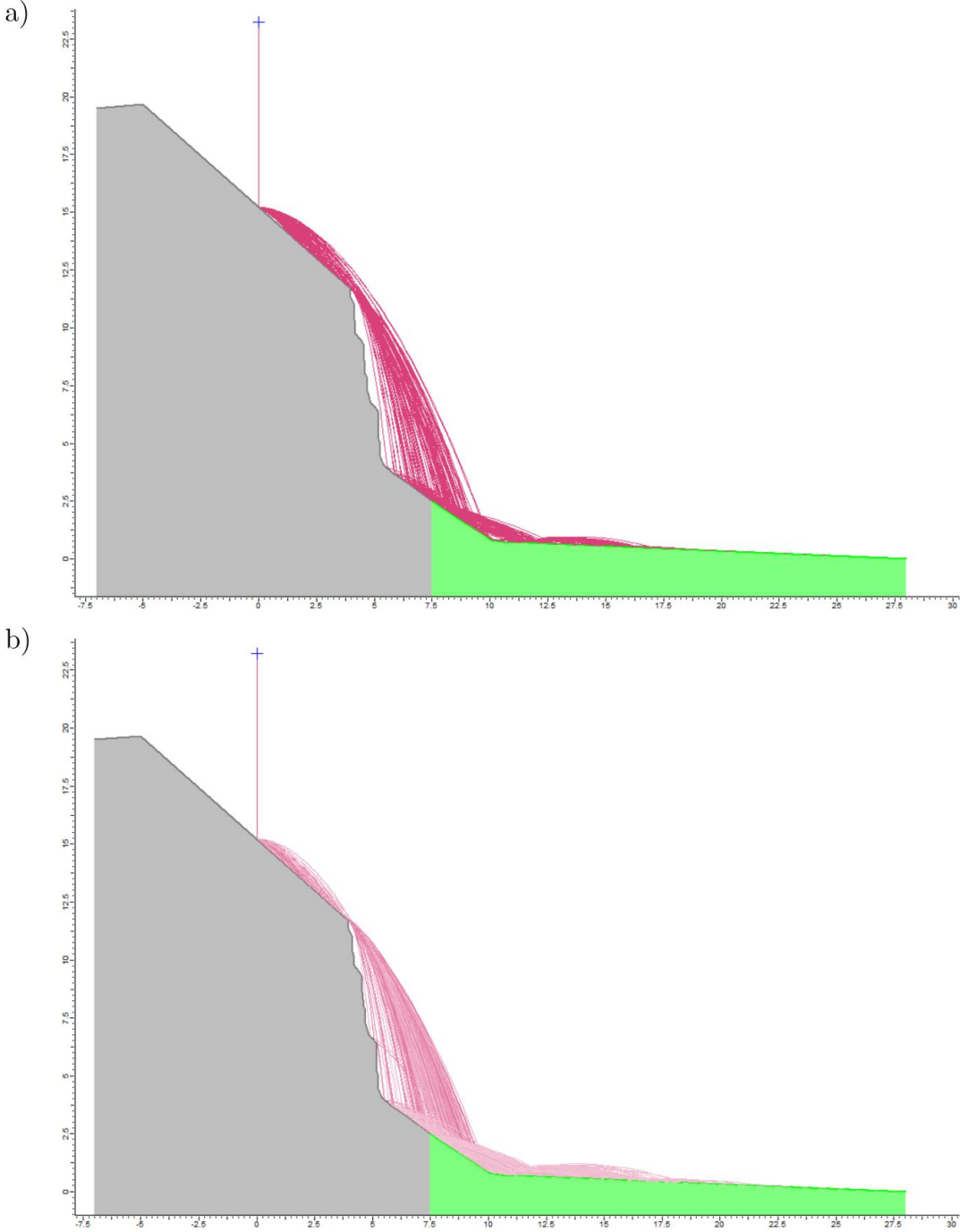
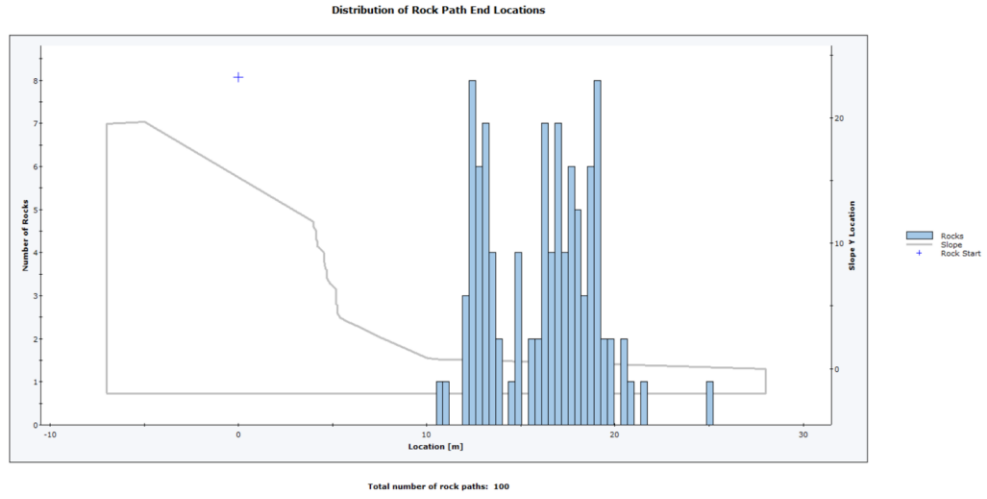


Figure 3-3 Trajectories results for the in-situ simulations: a) unfragmented and b) fragmented.

a)



b)

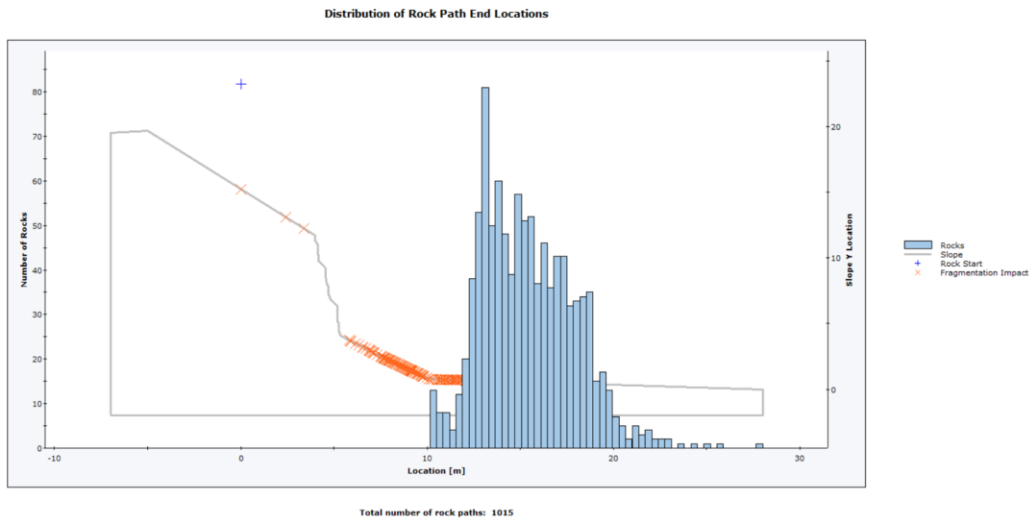
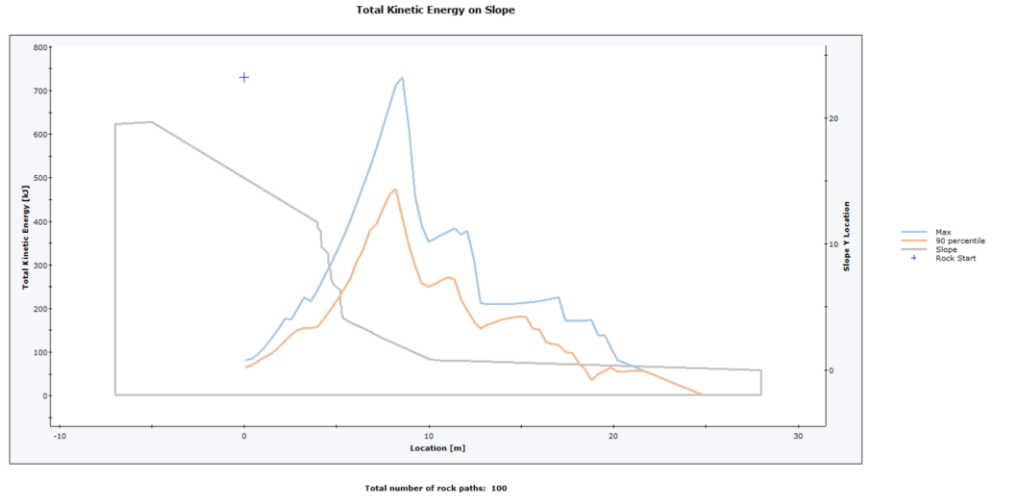


Figure 3-4 Endpoint location results for the in-situ simulations: a) unfragmented and b) fragmented.

a)



b)

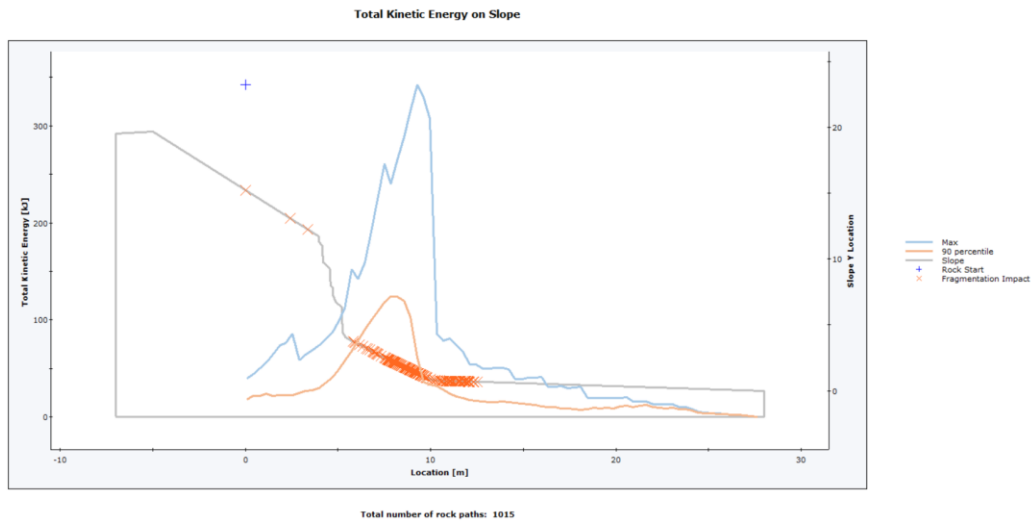


Figure 3-5 Total and 90<sup>th</sup> percentile kinetic energy results for the in-situ simulations: a) unfragmented and b) fragmented.

### 3.1. Comparison with in-situ observation

The comparison between the simulation and the in-situ test was made in terms of the number of fragments with mass > 0.01 kg and their runout distances. During the calibration phase, 24 blocks were simulated to match the observed fragment count above this threshold. Matas et al. (2020) reported about 250 fragments, while the RocFall2 simulation produced 242 fragments under the same conditions.

Figure 3-6 shows the runout distribution of fragments measured in the field (Matas et al., 2020) and predicted by RocFall2. Approximately 85% of the fragments from the in-situ tests stopped within 20 m of the first impact point on the inclined slope, compared to 96% in the simulation. This discrepancy likely stems from the irregular shape of real blocks and the simplified slope geometry in RocFall2 (2D profile vs 3D). Nevertheless, considering the assumptions underlying the fragmentation model proposed by Guccione et al. (2025), the simulation results can be considered acceptable.

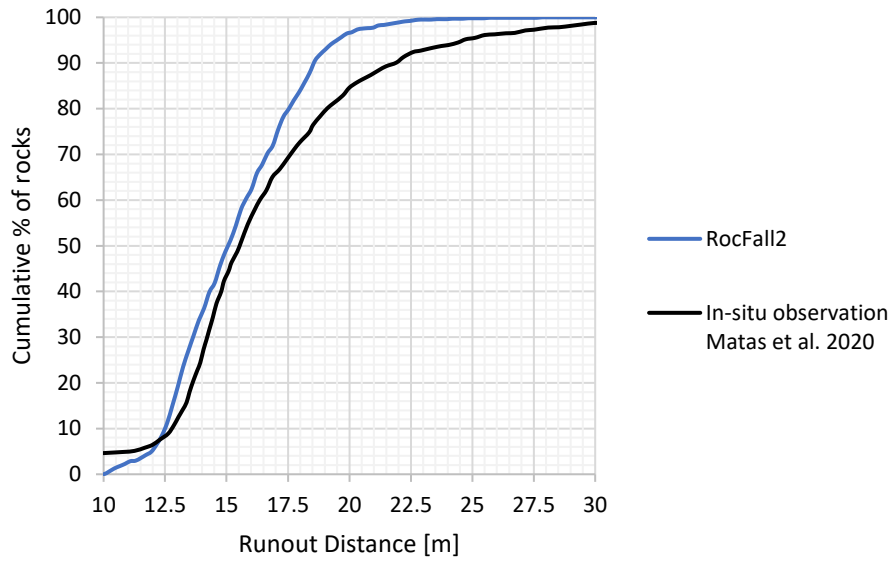


Figure 3-6 Comparison of fragment runout distances from RocFall2 simulations versus in-situ observations by Matas et al. 2020

# References

---

- Gili JA, Ruiz-Carulla R, Matas G, Moya J, Prades A, Corominas J, Lantada N, Núñez-Andrés MA, Buill F, Puig C, Martínez-Bofill J, Saló L, Mavrouli O (2022) Rockfalls: analysis of the block fragmentation through field experiments. *Landslides*. <https://doi.org/10.1007/s10346-021-01837-9>
- Guccione DE, Buzzi O, Thoeni K, Fityus S, Giacomini A (2021a) Predicting the fragmentation survival probability of brittle spheres upon impact from statistical distribution of material properties. *Int J Rock Mech Min Sci*. 142:104768. <https://doi.org/10.1016/j.ijrmms.2021.104768>
- Guccione DE, Thoeni K, Fityus S, Nader F, Giacomini A, Buzzi O (2021b) An experimental setup to study the fragmentation of rocks upon impact. *Rock Mech Rock Eng*. <https://doi.org/10.1007/s00603-021-02501-3>
- Guccione DE, Buzzi O, Thoeni K, Giacomini A, Fityus S (2022) Practical considerations for the application of a survival probability model for rockfall. *Aust Geomech J* 57(2):115–129
- Guccione DE, Giacomini A, Thoeni K, Fityus S, Buzzi O (2023) On the dynamic fragmentation of rock-like spheres: insights into fragment distribution and energy partition. *Rock Mech Rock Eng* 56(2):847–873. <https://doi.org/10.1007/s00603-022-03114-0>
- Guccione DE, Barros G, Thoeni K, Huang Z, Giacomini A, Buzzi O (2025). A new stochastic rockfall fragmentation approach for lumped mass simulations. *Rock Mech Rock Eng*. <https://doi.org/10.1007/s00603-025-04743-x>
- Matas G, Lantada N, Corominas J, Gili J, Ruiz-Carulla R, Prades A. (2020). Simulation of Full-Scale Rockfall Tests with a Fragmentation Model. *Geosciences*, 10(5), 168. <https://www.mdpi.com/2076-3263/10/5/168>
- Prades-Valls A, Corominas J, Lantada N, Matas G, Nunez-Andres MA (2022) Capturing rockfall kinematic and fragmentation parameters using high-speed camera system. *Eng Geol*. 302:106629. <https://doi.org/10.1016/j.enggeo.2022.106629>